

TRKM: Twin Restricted Kernel Machines for Classification and Regression

A. Qadir^a, M. Tanveer^{a,*}

^a*Department of Mathematics, Indian Institute of Technology Indore, Simrol, Indore, 453552, Madhya Pradesh, India*

Abstract

Restricted kernel machines (RKMs) have considerably improved generalization in machine learning. Recent advancements explored various techniques within the RKM framework, integrating kernel functions with least squares support vector machines (LSSVM) to mirror the energy function of restricted Boltzmann machines (RBM), leading to enhanced performance. However, RKMs may face challenges in generalization when dealing with unevenly distributed or complexly clustered data. Additionally, as the dataset size increases, the computational burden of managing high-dimensional feature spaces can become substantial, potentially hindering performance in large-scale datasets. To address these challenges, we propose twin restricted kernel machine (TRKM). TRKM combines the benefits of twin models with the robustness of the RKM framework to enhance classification and regression tasks. By leveraging the Fenchel-Young inequality, we introduce a novel conjugate feature duality, allowing the formulation of classification and regression problems in terms of dual variables. This duality provides an upper bound to the objective function of the TRKM problem, resulting in a new methodology under the RKM framework. The model uses an energy function similar to that of RBM, incorporating both visible and hidden variables corresponding to both classes. Additionally, the kernel trick is employed to map data into a high-dimensional feature space, where the model identifies an optimal separating hyperplane using a regularized least squares approach. Extensive experiments conducted on a diverse range of datasets from UCI, and KEEL confirm the superiority of TRKM over existing baseline models, demonstrating its effectiveness in handling complex data structures with improved robustness and efficiency. Furthermore, we implemented the proposed TRKM model to the brain age estimation dataset. Experimental results highlight the model's effectiveness in predicting brain age prediction.

Keywords: Restricted Boltzmann machines, Kernel methods, Restricted kernel machines, Twin support vector machine, Brain age estimation.

*Corresponding author

Email addresses: mscphd2207141002@iiti.ac.in (A. Qadir), mtanveer@iiti.ac.in (M. Tanveer)

1. Introduction

Support vector machines (SVMs) [1] have emerged as a powerful tool for solving classification problems. SVMs are based on statistical learning theory and the principle of maximizing the margin to identify the optimal hyperplane that separates classes, achieved by solving a quadratic programming problem (QPP). SVM has been extensively applied to a wide range of real-world challenges, such as remote sensing [2], EEG signal classification [3], diagnosis of Alzheimer's disease [4], feature extraction [5], and so on. SVM offers significant advantages by employing the structural risk minimization (SRM) principle, which enhances generalization and reduces errors during the training phase. However, it faces challenges in real-world applications due to its high computational complexity. Least squares SVM (LSSVM) was proposed by Suykens and Vandewalle [6] to address the computational burden of SVM. Unlike SVM, LSSVM uses a quadratic loss function rather than a hinge loss function, enabling the use of equality constraints in the classification problem. As a result, the solution can be obtained by solving a system of linear equations, thereby avoiding the need to solve large QPP. LSSVM has significantly lower computation time than SVM, making it more efficient for large-scale problems. Over the past decade, significant progress has been made in enhancing the accuracy of SVM. One notable development is the generalized eigenvalue proximal SVM (GEPSVM) introduced by Mangasarian and Wild [7], and the twin SVM (TSVM), proposed by Jayadeva et al. [8]. GEPSVM addresses the generalized eigenvalue problem, avoiding the need to solve a QPP. However, TSVM is four times faster than standard SVM because it solves two smaller QPPs rather than a single large QPP [8, 9] and establishing it as a notable and superior alternative. In order to keep each hyperplane near to the data points of one class and at least one unit away from the data points of the other class, TSVM generates a pair of non-parallel hyperplanes. Recently, several variants of TSVM have been introduced, such as the enhanced feature based granular ball TSVM (EF-GBT SVM) [10], least squares TSVM (LST SVM) [11], intuitionistic fuzzy universum TSVM for imbalanced data (IFUT SVM-ID)[12], IF generalized eigenvalue proximal SVM (IF-GEPSVM) [13] multiview learning with twin parametric margin SVM (MvTPMSVM) [14], multiview SVM with wave loss (Wave-MvSVM) [15] and many more.

While SVM and its variants are effectively applied to regression tasks, they are referred to as support vector regression (SVR) [16]. In contrast to SVM, SVR generates a tolerance margin ϵ and seeks for the best hyperplane to minimize the error within it. Thus, SVR identifies a function where the error can be up to ϵ distance, meaning any error within ϵ deviation from the true values is considered acceptable. SVR learns at a relatively slow pace because it requires solving a QPP. Researchers have developed many variants of SVR to boost its performance by lowering computational complexity and increasing accuracy [17, 18]. SVR involves high computational costs, which led to the development of the efficient twin SVR

(TSVR) [19]. TSVR utilizes ϵ -insensitive upper and lower bounds to refine and optimize the final regression function. Its formulation is more computationally efficient, as it requires solving two smaller QPPs, leading to a substantial increase in speed compared to SVR. Further, several variants of TSVR have been proposed, including twin projection SVR [20], ϵ -TSVR [21], and twin support vector quantile regression (TSVQR) [22], and so on. The previously described variations solve a pair of QPPs, which may need a significant amount of memory and time. Zhao et al. [23] proposed twin least squares SVR (TLSSVR), to address this high computational burden. TLSSVR replaces the inequality constraints of TSVR with equality constraints, which allows the model to be trained by solving a system of linear equations.

Both linear SVM and SVR, along with their variants, generate only linear decision boundaries. Consequently, if the data is not linearly separable, these models may have difficulty accurately classifying the data points. In contrast, kernel-based SVM [24] and SVR [16] have made a significant impact across various application domains by effectively managing complex data structures, enabling them to handle non-linear relationships and improve classification and regression performance [25, 26]. Kernel functions implicitly allow SVM and SVR to operate in a high-dimensional feature space, which permits them to capture non-linear relationships between features. This flexibility makes kernel-based SVM and SVR highly versatile, effectively handling a broad spectrum of data types and structures [27]. Despite their robust mathematical foundations, kernel methods face challenges when scaling to large datasets. Additionally, selecting the appropriate kernel function and tuning its parameters is a complex task, requiring careful consideration and optimization to achieve the best performance. Additionally, Suykens [28] introduced restricted kernel machine (RKM) for classification and regression, aiming to integrate kernel methods with neural network approaches. This development extends the utility of kernel techniques, enabling them to tackle more complex real-world problems effectively. RKM provides a representation of LSSVM that mimics the energy function of the restricted Boltzmann machine (RBM) [29] by employing the Legendre-Fenchel duality [30]. Although RKM has been effectively used in generative models [31, 32], classification [33], and disentangled representations [34]. RKM generates a non-linear separating hyperplane that can efficiently handle non-linear relationships by using the kernel method to convert data into a high-dimensional feature space. However, as the dataset size increases, the computational demands of managing high-dimensional spaces can become significant, leading to potential performance issues in large-scale datasets. Motivated by the advantages of TSVM and LSTVM, and considering the computational and generalization challenges RKM faces, we propose the twin restricted kernel machine (TRKM). This model integrates the principles of RKM with the benefits of twin methods, offering an improved approach for classification and regression tasks. By leveraging the kernel trick and addressing the computational complexities associated with large

datasets, TRKM aims to enhance performance while maintaining efficiency. To the best of our knowledge, this is the first time that the RKM framework is being utilized in a twin variant for both classification and regression, aimed at improving robustness and efficiency in handling complex data structures. The main contributions of our work are as follows:

1. Building on the strengths of TSVM and LSTSVM, and addressing the computational and generalization challenges encountered with RKM, we proposed the twin restricted kernel machine (TRKM). TRKM model combines the foundational principles of RKM with the advantages of twin methods, offering a robust solution for both classification and regression tasks.
2. TRKM adopts an energy function akin to that used in restricted Boltzmann machines (RBM), integrating both visible and hidden variables within a non-probabilistic framework to capture complex patterns.
3. In TRKM, the kernel trick is utilized to project data into a high-dimensional feature space. Within this space, the proposed model identifies a hyperplane that optimally separates the training instances through a regularized least squares approach, enhancing the model’s performance and adaptability.
4. We introduce a novel conjugate feature duality based on the Fenchel-Young inequality, enabling the expression of classification and regression problems in terms of conjugate dual variables. This duality provides an upper bound on the objective function of the TRKM problem for both classification and regression, resulting in a new methodology within the RKM framework for these tasks.
5. We conducted experiments on 36 real-world datasets from UCI [35] and KEEL [36] repository. Numerical experiments and statistical analyses reveal that the proposed TRKM model outperforms the baseline models.
6. We conducted experiments on the brain age dataset to assess the effectiveness of the proposed TRKM model. The empirical findings provide strong evidence of the TRKM model’s suitability for the early detection of AD using brain age as a biomarker.

2. Related Works

This section presents the notations used in this paper, along with a brief overview of TSVM, TSVR, and the proposed RKM model for classification and regression.

2.1. Notations

Consider a classification dataset denoted by \mathcal{T} , consisting of pairs (x_i, y_i) where $x_i \in \mathbb{R}^{1 \times m}$ is a feature vector with m features and $y_i \in \{+1, -1\}$ is the class label, with $+1$ indicating the positive class and -1

indicating the negative class. The positive class feature vectors are collected into an $n_1 \times m$ matrix A , where n_1 is the number of positive samples, and the negative class feature vectors are collected into an $n_2 \times m$ matrix B , where n_2 is the number of negative samples. Here, $n = n_1 + n_2$ represents the total number of samples in the dataset.

Consider a regression dataset denoted by \mathcal{M} , consisting of pairs (u_i, t_i) where $u_i \in \mathbb{R}^{1 \times m}$ is a feature vector with m features and $t_i \in \mathbb{R}$ is the corresponding continuous output value. The feature vectors u_i are organized into an $n \times m$ matrix X , where n is the total number of samples, and the output values t_i are organized into an $n \times 1$ vector Y . Here, n represents the total number of samples in the regression dataset.

2.2. Twin Support Vector Machine (TSVM)

In TSVM [8], two non-parallel hyperplanes are generated. Each hyperplane passes through the samples of its respective class and aims to maximize the margin between the hyperplanes and the samples of the opposing class. The optimization problem for TSVM can be formulated as follows:

$$\begin{aligned}
& \min_{w_1, b_1} \frac{1}{2} \|\mathcal{K}(A, C^T)w_1 + e_1 b_1\|^2 + d_1 e_2^T \xi_2 \\
& \text{s.t.} \quad -(\mathcal{K}(B, C^T)w_1 + e_2 b_1) + \xi_2 \geq e_2, \\
& \quad \quad \xi_2 \geq 0,
\end{aligned} \tag{1}$$

and

$$\begin{aligned}
& \min_{w_2, b_2} \frac{1}{2} \|\mathcal{K}(B, C^T)w_2 + e_2 b_2\|^2 + d_2 e_1^T \xi_1 \\
& \text{s.t.} \quad (\mathcal{K}(A, C^T)w_2 + e_1 b_2) + \xi_1 \geq e_1, \\
& \quad \quad \xi_1 \geq 0,
\end{aligned} \tag{2}$$

where d_1 and d_2 (> 0) are penalty parameters, e_1 and e_2 are column vectors of ones with appropriate dimensions, \mathcal{K} is kernel function and ξ_1 and ξ_2 are slack vectors, respectively.

2.3. Twin Support Vector Regression (TSVR)

TSVR extends the concept of TSVM to regression problems. In TSVR, two separate regression functions are learned, each focusing on approximating different parts of the data distribution. By solving two QPPs simultaneously, TSVR aims to find two distinct regression functions that minimize the prediction error while maintaining a balance between the models. The optimization problem of TSVR is given as

follows:

$$\begin{aligned}
& \min_{w_1, b_1} \frac{1}{2} \|Y - e\epsilon_1 - (\mathcal{K}(X, X^T)w_1 + e_1 b_1)\|^2 + d_1 e^T \xi_2 \\
& \text{s.t. } Y - (\mathcal{K}(X, X^T)w_1 + e b_1) + \xi_2 \geq e\epsilon_1, \\
& \quad \xi_2 \geq 0,
\end{aligned} \tag{3}$$

and

$$\begin{aligned}
& \min_{w_2, b_2} \frac{1}{2} \|Y + e\epsilon_2 - (\mathcal{K}(X, X^T)w_2 + e b_2)\|^2 + d_2 e^T \xi_1 \\
& \text{s.t. } (\mathcal{K}(X, X^T)w_2 + e_1 b_2) - Y + \xi_1 \geq e\epsilon_2, \\
& \quad \xi_1 \geq 0,
\end{aligned} \tag{4}$$

where d_1 and d_2 (> 0) are regularization parameters, ξ_1 and ξ_2 are slack vectors, respectively. Therefore, the regression function of a nonlinear TSVR can be expressed as:

$$\begin{aligned}
f(x) &= \frac{1}{2}(f_1(x) + f_2(x)) \\
&= \frac{1}{2}((w_1 + w_2)^T \mathcal{K}(x, X^T)) + \frac{1}{2}(b_1 + b_2).
\end{aligned} \tag{5}$$

2.4. Restricted Kernel Machine (RKM)

Here, we present an overview of the RKM model, as described by Suykens [28], which is closely related to the well-known LSSVM model [6]. RKM utilizes the kernel trick to transform the data into a high-dimensional feature space, enabling the construction of a linear separating hyperplane. The optimization problem for RKM is given as follows:

$$J = \frac{\gamma}{2} Tr(w^T w) + \sum_{i=1}^N (1 - (\phi(x_i)^T w + b)y_i)h_i - \frac{\eta}{2} \sum_{i=1}^N h_i^2, \tag{6}$$

where γ and η are the regularization parameters, b is the bias term, and h represents the hidden features. The solution to equation (6) is obtained by taking the partial derivatives of J with respect to (w.r.t.) w , b , and h_i , and then setting these derivatives to zero. For a detailed derivation, refer to Suykens [28]. The

solution to the optimization problem is given by:

$$\begin{bmatrix} \mathbf{1}_N & \frac{1}{\gamma}\mathcal{K} + \eta\mathbf{I}_N \\ 0 & \mathbf{1}_N^T \end{bmatrix} \begin{bmatrix} b \\ h \end{bmatrix} = \begin{bmatrix} y \\ 0 \end{bmatrix}, \quad (7)$$

where \mathcal{K} is the kernel matrix, $\mathbf{1}_N$ denotes a column vector with all its entries equal to one, \mathbf{I}_N is the identity matrix and $h \in \mathbb{R}^{N \times 1}$.

3. Proposed Twin Restricted Kernel Machines for Classification (TRKM-C)

This section provides a detailed explanation of the proposed TRKM for classification (TRKM-C). We begin by outlining the general mathematical framework of the TRKM-C. TRKM-C presents a distinctive approach to kernel methods by integrating both visible and hidden variables. This method is analogous to the energy function found in RBM [29], thereby establishing a connection between kernel methods and RBM. TRKM-C can be associated with the energy form expression of an RBM, interpreted through hidden h_1 (h_2) and visible units v_1 (v_2) corresponding to +1 (-1) class. Similar to RBM, TRKM-C is characterized by a scalar-valued energy function in both the training and prediction phases. Consistent with kernel methods, the optimal solutions for this objective function are obtained by solving a linear system or performing matrix decomposition in both the training and prediction phases.

Assume that the function $\phi : x_i \rightarrow \phi(x_i)$ maps the training samples from the input space to a high-dimensional feature space during both the training and prediction phases. The formulation of TRKM-C for the first hyperplane is given as follows:

$$\begin{aligned} \min_{w_1, \xi_1} J_1(w_1, \xi_1) = & \min_{w_1, \xi_1} \frac{\gamma_1}{2} Tr(w_1^T w_1) + e_2^T (\phi(B)w_1 + e_2 b_1) + \frac{1}{2\eta_1} \xi_1^T \xi_1 \\ \text{s.t. } & \xi_1 = e_1 - \phi(A)w_1 - e_1 b_1, \end{aligned} \quad (8)$$

where w_1 is the interconnection matrix, ξ_1 is the error vector, b_1 denotes the bias term, the vectors e_1 and e_2 are ones of the suitable dimensions, and γ_1 and η_1 are the tunable parameters, respectively. The connection between LSSVM and RBM in TRKM-C is formed by applying the Legendre-Fenchel conjugate for quadratic functions [30]. The TRKM-C establishes an upper bound for J_1 by incorporating the hidden layer representations h_1 as follows:

$$\frac{1}{2\eta_1} \xi_1^T \xi_1 \geq \xi_1^T h_1 - \frac{\eta_1}{2} h_1^T h_1, \quad \forall \xi_1, h_1. \quad (9)$$

Combining (8) and (9) leads to

$$J_1 \geq \xi_1^T h_1 - \frac{\eta_1}{2} h_1^T h_1 + \frac{\gamma_1}{2} Tr(w_1^T w_1) + e_2^T (\phi(B)w_1 + e_2 b_1)$$

$$\text{s.t. } \xi_1 = e_1 - \phi(A)w_1 - e_1 b_1. \quad (10)$$

The tight upper bound of J_1 can be obtained by incorporating the constraints as follows:

$$J_1 \geq (e_1 - \phi(A)w_1 - e_1 b_1)^T h_1 - \frac{\eta_1}{2} h_1^T h_1 + \frac{\gamma_1}{2} Tr(w_1^T w_1) + e_2^T (\phi(B)w_1 + e_2 b_1)$$

$$= \hat{J}_1. \quad (11)$$

Now, examine the stationary points of \hat{J}_1 by taking the gradients w.r.t. w_1 , h_1 , and b_1 as follows:

$$\frac{\partial \hat{J}_1}{\partial w_1} = 0 \implies w_1 = \frac{1}{\gamma_1} (\phi(A)^T h_1 - \phi(B)^T e_2), \quad (12)$$

$$\frac{\partial \hat{J}_1}{\partial h_1} = 0 \implies \eta_1 h_1 = e_1 - \phi(A)w_1 - e_1 b_1, \quad (13)$$

$$\frac{\partial \hat{J}_1}{\partial b_1} = 0 \implies h_1^T e_1 = e_2^T e_2. \quad (14)$$

Substituting the weight vector w_1 from Eq (12) into (13), we obtain:

$$\frac{1}{\gamma_1} \phi(A) \phi(A)^T h_1 - \frac{1}{\gamma_1} \phi(A) \phi(B)^T e_2 + \eta_1 h_1 + b_1 e_1 = e_1. \quad (15)$$

By calculating the stationary points of the objective function, we obtain the following system of linear equations:

$$\left[\begin{array}{c|c} \frac{1}{\gamma_1} \mathcal{K}(A, A^T) + \eta_1 I & e_1 \\ \hline e_1^T & 0 \end{array} \right] \begin{bmatrix} h_1 \\ b_1 \end{bmatrix} = \begin{bmatrix} e_1 + \frac{1}{\gamma_1} \mathcal{K}(A, B^T) e_2 \\ e_2^T e_2 \end{bmatrix}, \quad (16)$$

where I represents a matrix of ones of appropriate dimension, and \mathcal{K} represents the kernel function.

The optimization problem of TRKM-C for the second hyperplane is given as follows:

$$\min_{w_2, \xi_2} J_2(w_2, \xi_2) = \min_{w_2, \xi_2} \frac{\gamma_2}{2} Tr(w_2^T w_2) - e_1^T (\phi(A)w_2 + e_1 b_2) + \frac{1}{2\eta_2} \xi_2^T \xi_2$$

$$\text{s.t. } \xi_2 = -e_2 - \phi(B)w_2 - e_2 b_2. \quad (17)$$

The tight upper bound of J_2 can be obtained by incorporating the constraints as follows:

$$\begin{aligned} J_2 &\geq (-e_2 - \phi(B)w_2 - e_2b_2)^T h_2 - \frac{\eta_2}{2} h_2^T h_2 + \frac{\gamma_2}{2} \text{Tr}(w_2^T w_2) - e_1^T (\phi(A)w_2 + e_1b_2) \\ &= \hat{J}_2. \end{aligned} \quad (18)$$

Analogously, w_2 corresponding to the -1 class can be calculated by the subsequent equation:

$$w_2 = \frac{1}{\gamma_2} (\phi(B)^T h_2 + \phi(A)^T e_1). \quad (19)$$

By determining the stationary points of the objective for the -1 class, we obtain the following linear problem:

$$\left[\begin{array}{c|c} \frac{1}{\gamma_2} \mathcal{K}(B, B^T) + \eta_2 I & e_2 \\ \hline e_2^T & 0 \end{array} \right] \begin{bmatrix} h_2 \\ b_2 \end{bmatrix} = - \begin{bmatrix} e_2 + \frac{1}{\gamma_2} \mathcal{K}(B, A^T) e_1 \\ e_1^T e_1 \end{bmatrix}. \quad (20)$$

Once the optimal values of h_1 (b_1) and h_2 (b_2) are calculated for the $+1$ and -1 class, respectively. To predict the label of a new sample x , the following decision function can be used as follows:

$$\text{class}(x) = \text{sign}(f_1(x) + f_2(x)), \quad (21)$$

where

$$f_1(x) = \frac{1}{\gamma_1} [\mathcal{K}(x, A^T) h_1 - \mathcal{K}(x, B^T) e_2] + b_1, \quad (22)$$

and

$$f_2(x) = \frac{1}{\gamma_2} [\mathcal{K}(x, B^T) h_2 + \mathcal{K}(x, A^T) e_1] + b_2. \quad (23)$$

Algorithm 1 provides a concise description of the proposed TRKM-C algorithm.

4. Proposed Twin Restricted Kernel Machines for Regression (TRKM-R)

This section provides a detailed detailed formulation of the proposed twin restricted kernel machines for regression (TRKM-R). TRKM-R can be related to the energy form expression of an RBM by interpreting it in terms of the hidden and visible units. This connection enables us to interpret TRKM-R using

a framework similar to RBMs, where the energy function captures the interactions between hidden and visible units. Given these parallels with RBMs and the absence of hidden-to-hidden connections, we refer to this specific interpretation of the model as a TRKM representation for regression. The first optimization problem of TRKM-R can be obtained as:

$$\begin{aligned} \min_{w_1, \xi_1} J_1(w_1, \xi_1) = & \min_{w_1, \xi_1} \frac{\gamma_1}{2} \text{Tr}(w_1^T w_1) - e^T (\phi(X)w_1 + eb_1) + \frac{1}{2\eta_1} \xi_1^T \xi_1 \\ \text{s.t. } & Y = \phi(X)w_1 + eb_1 - \xi_1. \end{aligned} \quad (24)$$

We derived the upper bound for J by applying the same property used in the classification problem, resulting in:

$$\begin{aligned} J_1 \geq & \xi_1^T h_1 - \frac{\eta_1}{2} h_1^T h_1 + \frac{\gamma_1}{2} \text{Tr}(w_1^T w_1) - e^T (\phi(X)w_1 + eb_1) \\ \text{s.t. } & Y = \phi(X)w_1 + eb_1 - \xi_1. \end{aligned} \quad (25)$$

The upper bound can be obtained by substituting the constraints:

$$\begin{aligned} J_1 \geq & (\phi(X)w_1 + eb_1 - Y)^T h_1 - \frac{\eta_1}{2} h_1^T h_1 + \frac{\gamma_1}{2} \text{Tr}(w_1^T w_1) - e^T (\phi(X)w_1 + eb_1) \\ = & \hat{J}_1. \end{aligned} \quad (26)$$

The stationary points of \hat{J}_1 are given by

$$\frac{\partial \hat{J}_1}{\partial w_1} = 0 \implies w_1 = \frac{1}{\gamma_1} (\phi(X)^T e - \phi(X)^T h_1), \quad (27)$$

$$\frac{\partial \hat{J}_1}{\partial h_1} = 0 \implies \eta_1 h_1 = \phi(X)w_1 + eb_1 - Y, \quad (28)$$

$$\frac{\partial \hat{J}_1}{\partial b_1} = 0 \implies h_1^T e = e^T e. \quad (29)$$

On employing w_1 in (28), we get

$$\frac{1}{\gamma_1} \phi(X)\phi(X)^T e - \frac{1}{\gamma_1} \phi(X)\phi(X)^T h_1 - \eta h_1 + eb_1 = Y, \quad (30)$$

Using Eqs (30) and (29), we can find the solution by solving the following system of linear equations:

$$\left[\begin{array}{c|c} \frac{1}{\gamma_1} \mathcal{K}(X, X^T) + \eta_1 I & -e \\ \hline e^T & 0 \end{array} \right] \begin{bmatrix} h_1 \\ b_1 \end{bmatrix} = \begin{bmatrix} -Y + \frac{1}{\gamma_1} \mathcal{K}(X, X^T) e \\ e^T e \end{bmatrix}. \quad (31)$$

The second optimization problem of TRKM-R can be obtained as follows:

$$\begin{aligned} \min_{w_2, \xi_2} J_2(w_2, \xi_2) &= \min_{w_2, \xi_2} \frac{\gamma_2}{2} \text{Tr}(w_2^T w_2) + e^T (\phi(X)w_2 + eb_2) + \frac{1}{2\eta_2} \xi_2^T \xi_2 \\ \text{s.t. } Y &= \phi(X)w_1 + eb_2 + \xi_2. \end{aligned} \quad (32)$$

By applying the constraints, we derive the following accurate upper bound for J_2 :

$$\begin{aligned} J_2 &\geq (Y - \phi(X)w_2 - eb_2)^T h_2 - \frac{\eta_2}{2} h_2^T h_2 + \frac{\gamma_2}{2} \text{Tr}(w_2^T w_2) + e^T (\phi(X)w_2 + eb_2) \\ &= \hat{J}. \end{aligned} \quad (33)$$

By taking the gradient of (33), we determine the weight vector associated with the second optimization problem:

$$w_2 = \frac{1}{\gamma_2} (\phi(X)^T h_2 - \phi(X)^T e). \quad (34)$$

Similarly, we can derive the following system of linear equations:

$$\left[\begin{array}{c|c} \frac{1}{\gamma_2} \mathcal{K}(X, X) + \eta_2 I & e \\ \hline e^T & 0 \end{array} \right] \begin{bmatrix} h_2 \\ b_2 \end{bmatrix} = \begin{bmatrix} Y + \frac{1}{\gamma_2} \mathcal{K}(X, X^T) e \\ e^T e \end{bmatrix}. \quad (35)$$

Once the optimal values of h_1 (b_1) and h_2 (b_2) are calculated. Then, we construct the estimated regressor as follows:

$$f(x) = (f_1(x) + f_2(x)) / 2, \quad (36)$$

where

$$f_1(x) = \frac{1}{\gamma_1} \mathcal{K}(x, X^T) (e - h_1) + b_1, \quad (37)$$

and

$$f_2(x) = \frac{1}{\gamma_2} \mathcal{K}(x, X^T)(h_2 - e) + b_2. \quad (38)$$

Algorithm 2 provides a concise description of the proposed TRKM-R algorithm.

Algorithm 1 Training and prediction of the proposed TRKM-C.

Require: Let $\{x_i\}_{i=1}^n$ be the input training dataset, A and B represent the matrix of +1 and -1 classes and the trade-off parameters $\gamma_1, \gamma_2, \eta_1$ and η_2 , respectively.

- 1: Find the kernel matrix $\mathcal{K}(A, A^T), \mathcal{K}(A, B^T), \mathcal{K}(B, B^T)$, and $\mathcal{K}(B, A^T)$.
 - 2: Calculate h_1, b_1 and h_2, b_2 corresponding to +1 and -1 class using Eqs (16) and (20).
 - 3: Find the decision function with dual representation using Eqs (22) and (23).
 - 4: The classification of a test sample x into class +1 or -1 is determined using Eq. (21).
-

Algorithm 2 Training and prediction of the proposed TRKM-R.

Require: Let X be the input training dataset, Y represent the vector that contains the input data's target values, and the trade-off parameters $\gamma_1, \gamma_2, \eta_1$ and η_2 , respectively.

- 1: Find the kernel matrix $\mathcal{K}(X, X^T)$.
 - 2: Calculate h_1, b_1 and h_2, b_2 using Eqs (31) and (35).
 - 3: Find the decision function with dual representation using Eqs (37) and (38).
 - 4: The predicted value of the new samples x is determined using Eq (36).
-

5. Experiments and Results

In this section, we conduct an extensive evaluation of the proposed TRKM model by performing experiments on UCI and KEEL datasets and comparing its performance with that of leading state-of-the-art models. Moreover, we use the Brain Age prediction dataset to evaluate the proposed models.

5.1. Experimental Setup

The experiments are conducted in Python 3.11 on Windows 11 running on a PC with system configuration Intel® Xeon® Gold 6226R CPU and 128 GB of RAM. The dataset is divided randomly in a 70 : 30 proportion, where 70% is allocated for training the model, and the remaining 30% is used for testing. We use five-fold cross-validation combined with a grid search method to fine-tune the model's hyperparameters, selecting the following ranges: $\eta_i = \gamma_i = \{10^{-5}, 10^{-4}, \dots, 10^5\}$ for $i = 1, 2$. We employ the Gaussian kernel, defined as $\mathcal{K}(x_i, x_j) = e^{-\frac{1}{2\sigma^2} \|x_i - x_j\|^2}$. The range $\{2^{-5}, 2^{-4}, \dots, 2^5\}$ is used to choose the Gaussian kernel parameter σ . For TRKM-C and TRKM-R, we adopt equal penalty parameters, *i.e.* $\eta_1 = \eta_2$ and $\gamma_1 = \gamma_2$, respectively. To assess the performance of the proposed TRKM-R model, we employ four metrics, including mean absolute error (*MAE*), root mean squared error (*RMS E*), negative error (*Neg Error*),

and positive error (*Pos Error*). The following are the specific definitions of these metrics:

$$RMSE = \sqrt{\frac{1}{n} \sum_{i=1}^n (f(x_i) - y_i)^2}, \quad (39)$$

$$MAE = \frac{1}{n} \sum_{i=1}^n |(f(x_i) - y_i)|, \quad (40)$$

$$Pos\ Error = \frac{1}{n} \sum_{i=1, f(x_i) \leq y_i}^n |(f(x_i) - y_i)|, \quad (41)$$

$$Neg\ Error = \frac{1}{n} \sum_{i=1, f(x_i) > y_i}^n |(f(x_i) - y_i)|. \quad (42)$$

5.2. Experimental Results and Statistical Analysis on UCI and KEEL Datasets for Classification

In this subsection, we offer a thorough comparison of the proposed TRKM-C model against the SVM [1], TSVM [8], Pin-GTSVM [37], RKM [28], and GBTSVM [38] models. 36 benchmark datasets from the KEEL and UCI repositories are used in this comparison. Optimal parameters and the average classification accuracy (ACC) of the proposed TRKM-C, along with the baseline SVM, TSVM, Pin-GTSVM, RKM, and GBTSVM models, are presented in Table 1. The ACC comparison demonstrates that our proposed TRKM-C model outperforms the baseline SVM, TSVM, Pin-GTSVM, RKM, and GBTSVM models on most of the datasets. The proposed TRKM-C model provides an average ACC of 90.85%, whereas the average ACC of SVM, TSVM, Pin-GTSVM, RKM, and GBTSVM models are 76.27%, 84.83%, 85.95%, 88.52%, and 88.74 respectively. The proposed TRKM-C model achieves a higher average ACC compared to the existing models. Average accuracy can sometimes be misleading if a model performs exceptionally well on one dataset but poorly across others. This can skew the results and may not provide a complete picture of the model's performance. To gauge the effectiveness and performance of the models, we employ the ranking method outlined by Demšar [39]. In this method, classifiers are ranked such that models with better performance receive lower ranks, while those with poorer performance are assigned higher ranks. The rank of the j^{th} model on the i^{th} dataset is expressed as \mathfrak{R}_j^i in order to evaluate p models over N datasets. The average rank of the model is determined as $\mathfrak{R}_j = \frac{1}{N} \sum_{i=1}^N \mathfrak{R}_j^i$. The average rank of the proposed TRKM-C along with the baselines SVM, TSVM, Pin-GTSVM, RKM, and GBTSVM models are 2.20, 4.98, 4.00, 3.86, 2.77 and 3.16, respectively. The lowest average rank is attained by the proposed TRKM-C model, indicating the most favorable position compared to the existing models. The Friedman test [39] is then used to determine whether the models differ significantly from one another. Under the null hypothesis of the Friedman test, it is assumed that all models have the same average rank, indicating equivalent performance.

Table 1: Classification ACC of the proposed TRKM-C and the baseline models across the real world datasets i.e. UCI and KEEL.

Model → Dataset ↓ (#Samples × #Feature)	SVM [1] ACC (%) (d_1, σ)	TSVM [8] ACC (%) (d_1, d_2, σ)	Pin-GTSVM [37] ACC (%) (d_1, d_2, τ, σ)	RKM [28] ACC (%) (γ, η, σ)	GBT SVM [38] ACC (%) (d_1, d_2, σ)	TRKM-C [†] ACC (%) (γ_1, η_1, σ)
aus (690 × 15)	56.25 ($10^{-5}, 2^{-5}$)	81.25 ($10^{-5}, 10^{-5}, 2^{-5}$)	79.33 ($10^2, 10^4, 0.1, 2^3$)	88.94 ($10^1, 10^3, 2^4$)	87.98 ($10^{-1}, 1, 2^5$)	87.5 ($10^{-1}, 10^{-3}, 2^2$)
breast_cancer (286 × 10)	74.42 ($10^{-5}, 2^{-5}$)	67.44 ($10^{-1}, 10^{-2}, 2^{-4}$)	63.95 ($10^2, 10^{-2}, 1, 2^{-4}$)	75.58 ($10^1, 10^{-3}, 2^4$)	62.79 ($10^1, 10^1, 2^5$)	77.91 ($10^{-1}, 10^{-1}, 2^2$)
checkerboard_Data (690 × 15)	56.25 ($10^{-5}, 2^{-5}$)	81.25 ($10^{-2}, 10^{-2}, 2^{-5}$)	79.33 ($10^{-1}, 10^{-5}, 0.5, 2^{-3}$)	86.94 ($10^1, 10^3, 2^4$)	87.98 ($10^{-1}, 1, 2^5$)	87.5 ($10^{-1}, 10^{-3}, 2^2$)
chess_krvkp (3196 × 37)	52.35 ($10^{-3}, 2^3$)	90.41 ($10^{-1}, 10^1, 2^{-5}$)	90.41 ($10^{-5}, 10^{-5}, 0.1, 2^4$)	98.27 ($10^{-1}, 10^{-5}, 2^5$)	97.08 (1, 1, 2 ⁵)	98.75 ($10^{-2}, 10^{-5}, 2^5$)
crossplane130 (130 × 3)	51.28 ($10^{-3}, 2^4$)	100 ($10^{-5}, 10^{-5}, 2^{-5}$)	97.44 ($10^{-1}, 10^{-3}, 1, 2^{-2}$)	100 ($10^{-5}, 10^4, 2^{-3}$)	100 ($10^{-5}, 10^{-5}, 2^5$)	100 ($10^{-5}, 10^{-5}, 2^{-5}$)
ecoli-0-1_vs_5 (240 × 7)	94.44 (1, 1)	97.22 ($10^{-5}, 10^{-4}, 2^{-3}$)	95.83 ($10^{-3}, 10^{-5}, 0.75, 2^4$)	96.81 ($10^2, 10^{-5}, 2^1$)	98.89 ($10^{-4}, 10^{-5}, 2^5$)	97.74 ($10^{-1}, 10^{-5}, 2^2$)
ecoli-0-1_vs_2-3-5 (244 × 8)	91.89 (1, 1)	90.59 ($10^{-4}, 10^{-3}, 2^5$)	94.59 ($10^{-5}, 10^{-5}, 0.1, 2^3$)	94.59 ($10^2, 10^2, 2^4$)	90.81 ($10^{-2}, 1, 2^2$)	93.24 ($10^{-5}, 10^4, 2^{-2}$)
ecoli-0-1-4-7_vs_2-3-5-6 (336 × 8)	87.13 ($10^{-5}, 2^{-5}$)	96.04 ($10^{-1}, 1, 2^{-1}$)	95.05 ($10^{-5}, 10^{-5}, 0.1, 2^2$)	93.55 ($10^{-4}, 10^2, 2^{-1}$)	96.67 (1, $10^{-1}, 2^2$)	96.67 ($10^{-5}, 10^{-5}, 2^{-5}$)
ecoli-0-1-4-7_vs_5-6 (332 × 7)	91 ($10^1, 1$)	96 ($10^{-3}, 10^{-2}, 2^2$)	96 ($10^{-1}, 10^{-5}, 0.5, 2^{-3}$)	98.36 ($10^{-5}, 10^{-5}, 1$)	94 (1, 1, 2 ⁵)	98.46 ($10^{-5}, 10^{-5}, 2^{-5}$)
ecoli-0-1-4-6_vs_5 (280 × 7)	98.81 (1, 1)	100 ($10^{-5}, 10^{-5}, 2^{-5}$)	100 ($10^{-5}, 10^{-5}, 0.1, 2^{-3}$)	98.81 ($10^{-5}, 10^1, 2^{-1}$)	97.62 (1, 1, 2 ⁵)	98.81 ($10^{-5}, 10^{-5}, 2^{-1}$)
haberman (306 × 4)	82.61 ($10^{-5}, 2^{-5}$)	75.35 (1, $10^{-1}, 2^{-3}$)	69.57 ($10^{-1}, 10^1, 1, 2^{-3}$)	76.09 ($10^{-1}, 10^1, 1$)	77.17 ($10^1, 1, 2^3$)	80.43 ($10^{-4}, 10^{-1}, 2^3$)
haberman_survival (306 × 4)	81.52 ($10^{-1}, 1$)	75.35 ($10^{-1}, 1, 2^{-2}$)	69.57 ($10^1, 10^{-1}, 1, 2^{-5}$)	76.09 ($10^{-1}, 10^1, 1$)	77.17 (1, $10^1, 2^2$)	80.43 ($10^{-3}, 10^{-1}, 2^3$)
heart_stat (270 × 14)	82.61 ($10^{-5}, 2^{-5}$)	79.35 (1, $10^{-1}, 2^{-5}$)	69.57 ($10^{-1}, 10^1, 1, 2^5$)	76.09 ($10^{-1}, 10^1, 1$)	79.35 ($10^1, 10^1, 2^5$)	80.43 ($10^{-4}, 10^{-1}, 2^3$)
led7digit-0-2-4-5-6-7-8-9_vs_1 (443 × 8)	56.79 ($10^{-5}, 2^{-5}$)	70.37 ($10^{-1}, 10^1, 2^{-5}$)	70.37 ($10^{-5}, 1, 0.25, 2^{-5}$)	87.65 ($10^1, 10^3, 2^4$)	79.01 ($10^{-5}, 10^{-5}, 2^5$)	85.19 ($10^{-2}, 10^{-2}, 2^3$)
mammographic (961 × 6)	81.95 (1, 1)	93.98 ($10^{-5}, 10^{-4}, 2^{-3}$)	93.98 ($10^{-5}, 1, 0.1, 2^{-5}$)	94.74 ($10^1, 10^{-5}, 2^2$)	94.74 ($10^{-5}, 10^{-5}, 2^5$)	94.98 ($10^{-2}, 10^{-4}, 2^{-5}$)
monks_3 (554 × 7)	52.94 ($10^{-5}, 2^{-5}$)	79.93 ($10^{-1}, 10^1, 2^{-5}$)	77.82 ($10^3, 10^{-5}, 1, 2^{-5}$)	78.74 ($10^{-1}, 10^{-3}, 2^4$)	81.31 ($10^{-1}, 10^{-1}, 2^5$)	79.24 ($10^{-5}, 10^{-5}, 2^{-2}$)
mushroom (8124 × 22)	46.11 ($10^{-5}, 2^{-5}$)	75.21 (1, $10^{-1}, 2^{-2}$)	95.81 ($10^1, 1, 0.25, 2^{-3}$)	49.1 ($10^5, 10^2, 2^{-5}$)	80.24 (1, $10^1, 2^5$)	80.84 ($10^2, 10^{-4}, 2^{-2}$)
musk_1 (476 × 167)	63.41 ($10^{-3}, 2^1$)	70.65 ($10^2, 10^3, 2^5$)	80.51 ($10^1, 10^2, 0.25, 2^{-3}$)	81.77 ($10^{-1}, 10^{-5}, 2^1$)	84.91 (1, $10^{-1}, 2^3$)	96.41 ($10^{-4}, 10^{-2}, 2^5$)
new_thyroid1 (215 × 16)	53.15 ($10^{-5}, 2^{-5}$)	83.15 ($10^{-5}, 10^{-5}, 2^{-5}$)	53.15 ($10^{-5}, 10^{-5}, 0.1, 2^{-1}$)	92.31 ($10^1, 10^{-5}, 2^5$)	91.61 ($10^{-1}, 1, 2^5$)	92.31 ($10^{-1}, 10^{-5}, 2^5$)
oocytes_merluccius_nucleus_4d (1022 × 42)	87.69 ($10^{-5}, 2^{-5}$)	98.46 ($10^{-2}, 10^{-2}, 2^{-3}$)	96.92 (1, $10^1, 0.75, 2^{-5}$)	98.46 (1, $10^3, 2^1$)	95.38 ($10^{-5}, 10^{-5}, 2^4$)	96.92 ($10^{-2}, 10^{-5}, 2^3$)
ozone (2536 × 6)	64.82 ($10^{-3}, 2^{-5}$)	76.22 ($10^{-2}, 10^1, 2^{-5}$)	79.48 (1, 1, 0.25, 2 ⁻⁴)	75.06 ($10^{-1}, 10^1, 2^5$)	77.2 (1, 1, 2 ⁴)	79.15 ($10^{-1}, 10^{-2}, 2^2$)
ringnorm (7400 × 21)	96.58 ($10^{-5}, 2^{-5}$)	96.58 ($10^{-5}, 10^{-5}, 2^{-5}$)	96.58 ($10^{-5}, 10^{-5}, 0.1, 2^{-3}$)	87.96 ($10^{-1}, 1, 2^5$)	94.09 ($10^1, 1, 2^5$)	97.58 ($10^{-2}, 10^{-2}, 2^3$)
shuttle-6_vs_2-3 (230 × 10)	90.42 (1, 2 ¹)	92.65 ($10^{-5}, 10^{-5}, 2^{-5}$)	93.06 ($10^{-5}, 10^{-5}, 0.1, 2^{-3}$)	89.07 ($10^{-2}, 10^{-5}, 2^1$)	96.94 ($10^1, 1, 2^5$)	96.44 ($10^{-3}, 10^{-5}, 1$)
spambase (4601 × 58)	95.65 ($10^{-5}, 2^{-5}$)	97.1 ($10^{-5}, 10^{-4}, 2^{-4}$)	97.1 ($10^{-5}, 10^{-5}, 0.1, 2^{-4}$)	100 ($10^{-5}, 10^5, 2^3$)	98.55 ($10^{-2}, 10^{-1}, 2^4$)	98.55 ($10^{-5}, 10^4, 1$)
spectf (267 × 45)	62.2 ($10^{-1}, 1$)	84.79 ($10^{-2}, 1, 2^{-3}$)	76.76 ($10^3, 10^4, 0.5, 2^3$)	79.37 ($10^2, 10^2, 2^4$)	90.88 ($10^1, 10^1, 2^5$)	98 ($10^{-5}, 10^3, 2^2$)
tic_tac_toe (958 × 10)	80.25 ($10^{-5}, 2^{-5}$)	79.42 ($10^{-1}, 10^{-1}, 2^{-5}$)	83.95 ($10^{-5}, 10^{-4}, 0.75, 2^{-3}$)	83.95 ($10^1, 1, 2^3$)	85.19 ($10^{-1}, 10^{-3}, 2^4$)	85.19 ($10^{-4}, 10^{-5}, 2^1$)
vehicle1 (846 × 19)	66.32 ($10^{-5}, 2^{-5}$)	95 ($10^{-1}, 10^{-2}, 2^{-2}$)	100 ($10^{-5}, 10^{-5}, 0.1, 2^2$)	100 ($10^{-5}, 10^3, 2^{-2}$)	98.96 ($10^1, 10^1, 2^4$)	99.65 ($10^{-1}, 10^{-3}, 2^5$)
vehicle2 (846 × 19)	75.98 ($10^{-5}, 2^{-5}$)	80.31 ($10^{-2}, 10^{-2}, 2^{-5}$)	77.95 ($10^{-2}, 1, 0.5, 2^3$)	88.58 ($10^{-1}, 1, 2^5$)	81.5 (1, 1, 2 ⁵)	81.89 ($10^{-3}, 1, 2^2$)
vertebral_column_2classes (310 × 7)	77.95 ($10^{-5}, 2^{-5}$)	76.46 ($10^{-2}, 10^1, 2^{-2}$)	96.06 ($10^{-2}, 1, 0.5, 2^5$)	98.82 (1, $10^5, 2^5$)	94.49 ($10^{-1}, 10^{-1}, 2^5$)	95.28 ($10^{-5}, 10^{-5}, 1$)
wdbc (194 × 34)	69.89 ($10^{-5}, 2^{-5}$)	89.25 ($10^{-3}, 10^{-2}, 2^{-5}$)	81.72 (1, 1, 0.25, 2 ⁻³)	89.25 (1, $10^5, 2^5$)	88.17 ($10^{-1}, 10^{-1}, 2^4$)	87.1 ($10^{-3}, 1, 2^1$)
yeast-0-2-5-6_vs_3-7-8-9 (1004 × 9)	77.97 ($10^{-5}, 2^{-5}$)	77.97 ($10^{-5}, 10^{-5}, 2^{-5}$)	77.97 ($10^{-5}, 10^{-5}, 0.1, 2^5$)	77.97 ($10^1, 10^{-1}, 2^4$)	76.27 ($10^{-5}, 10^{-5}, 2^5$)	76.27 ($10^{-3}, 1, 2^4$)
yeast-0-3-5-9_vs_7-8 (1004 × 9)	91.39 ($10^{-5}, 2^{-5}$)	84.04 ($10^{-1}, 10^1, 2^1$)	94.37 ($10^{-1}, 10^1, 0.75, 2^{-2}$)	94.04 ($10^2, 10^3, 2^4$)	94.04 (1, 1, 2 ⁵)	92.72 ($10^{-5}, 10^3, 2^{-1}$)
yeast-0-5-6-7-9_vs_4 (528 × 9)	87.5 ($10^{-5}, 2^{-5}$)	53.15 ($10^{-1}, 10^{-5}, 2^{-5}$)	95.7 ($10^2, 10^3, 0.1, 2^2$)	97.35 ($10^3, 10^4, 2^5$)	90.79 ($10^{-5}, 10^{-5}, 2^5$)	95.7 (1, $10^{-2}, 2^1$)
yeast-2_vs_4 (514 × 9)	91.19 ($10^{-5}, 2^{-5}$)	82.45 ($10^{-3}, 10^{-2}, 2^{-4}$)	88.68 ($10^5, 10^5, 0.1, 2^5$)	91.82 ($10^1, 1, 2^2$)	91.19 ($10^{-2}, 10^{-2}, 2^5$)	92.45 ($10^{-5}, 10^2, 2^{-1}$)
yeast3 (1484 × 9)	85.81 ($10^{-5}, 2^{-5}$)	94.19 ($10^{-1}, 10^1, 2^{-5}$)	94.19 ($10^{-2}, 1, 0.5, 2^2$)	96.77 ($10^1, 10^{-1}, 2^3$)	97.42 ($10^{-1}, 10^{-1}, 2^5$)	97.32 ($10^{-4}, 10^2, 1$)
Average ACC	76.27	84.83	85.95	88.52	88.74	90.85
Average Rank	4.98	4	3.86	2.77	3.16	2.20

[†] represents the proposed models.

The Friedman test follows a chi-squared distribution (χ_F^2) with $(p-1)$ degrees of freedom. Its calculation is given by: $\chi_F^2 = \frac{12N}{p(p+1)} \left[\sum_j \mathfrak{R}_j^2 - \frac{p(p+1)^2}{4} \right]$. The F_F statistic is calculated using the formula: $F_F = \frac{(N-1)\chi_F^2}{N(p-1)-\chi_F^2}$, where the F -distribution has $(p-1)$ and $(N-1) \times (p-1)$ degrees of freedom. For $p = 6$ and $N = 36$, we obtain $\chi_F^2 = 48.95$ and $F_F = 13.0732$ at the 5% significance level. According to the statistical F -distribution table, $F_F(5, 175) = 2.2657$. Since $F_F > 2.2657$, the null hypothesis is rejected. As a result, there is a statistically significant disparity among the models under comparison. The Nemenyi post hoc test is then used to assess the models' pairwise differences. The critical difference (C.D.) is calculated using the formula $\text{C.D.} = q_\alpha \sqrt{\frac{p(p+1)}{6N}}$, where q_α is the two-tailed Nemenyi test critical value obtained from the distribution table. With reference to the F -distribution table, the computed C.D. is 1.2567 at the 5% significance level, with $q_\alpha = 2.850$. The proposed TRKM-C model's average rank differences with the SVM, TSVM, Pin-GTSVM, RKM, and GBTSVM models are as follows: 2.78, 1.80, 1.66, 0.57 and 0.96, respectively. The Nemenyi post hoc test confirms that the proposed TRKM-C model is significantly superior to the baseline SVM, TSVM, and Pin-GTSVM models. The proposed TRKM-C model shows a statistically significant improvement over the RKM and GBTSVM models. Based on the lowest average rank attained by the TRKM-C model, we conclude that the proposed TRKM-C model excels in overall performance and ranking compared to existing models. Furthermore, to evaluate the model's performance, we use the

Table 2: Comparison of Win-Tie-Loss Results on UCI and KEEL classification datasets.

	SVM [1]	TSVM [8]	Pin-GTSVM [37]	RKM [28]	GBTSVM [38]
TSVM [8]	[24, 2, 10]				
Pin-GTSVM [37]	[28, 3, 5]	[11, 9, 16]			
RKM [28]	[29, 2, 5]	[22, 4, 10]	[25, 4, 7]		
GBTSVM [38]	[27, 1, 8]	[26, 2, 8]	[22, 0, 14]	[14, 3, 19]	
TRKM-C [†]	[31, 1, 4]	[30, 1, 5]	[26, 2, 8]	[20, 3, 13]	[24, 4, 8]

[†] represents the proposed models.

pairwise win-tie-loss sign test. Under the null hypothesis, the test assumes that two models perform equally well, each expected to be the best in half of the N datasets. A model is considered significantly superior if it surpasses the competition on approximately $N/2 + 1.96\sqrt{N/2}$ datasets. The two models are distributed equally if the number of ties between them is even. One tie is eliminated and the remaining ties are divided equally among the classifiers if the number of ties is odd. For $N = 36$, a model needs to secure at least 24 wins to demonstrate a significant difference from the other models. The proposed TRKM-C model is evaluated in comparison to the baseline models in Table 2. The entry $[x, y, z]$ in Table 2 shows that, when compared to the model listed in the column, the model listed in the row wins x times, ties y times, and loses z times. The proposed TRKM-C model demonstrates a statistically significant difference compared to the baseline models, with the exception of RKM. The TRKM-C model consistently demonstrates its superior

performance over the RKM model, as evidenced by its higher winning percentage. The results indicate that the proposed TRKM-C model considerably surpasses the performance of the baseline models.

5.3. Sensitivity Analysis on Real World UCI and KEEL Datasets for Classification

A comprehensive evaluation of the proposed TRKM-C model’s robustness requires analyzing its sensitivity to different hyperparameters. We conduct sensitivity analyses focusing on the following aspects: (1) η versus γ , and (2) η versus σ . We experiment with different ranges for each hyperparameter and assess their impact on the model’s performance.

1. A complete assessment of the robustness of the proposed TRKM-C model requires examining its sensitivity to the hyperparameters η and γ . This thorough investigation aids in determining the setup that optimizes predictive ACC and improves the model’s performance on unknown inputs. Fig 1 highlights significant fluctuations in model ACC across various η and γ values, demonstrating the sensitivity of the model to these hyperparameters. From Figs. 1a and 1b, the TRKM-C model performs best inside the ranges of η from 10^{-1} to 10^5 and γ from 10^{-5} to 10^{-1} . Also, Figs. 1c and 1d show that the model achieves maximum ACC when η and γ are within 10^{-5} to 10^3 . Therefore, we recommend using η and γ within the range of 10^{-5} to 10^{-1} for optimal results. However, fine-tuning may be required depending on the specific characteristics of the dataset to achieve the best generalization performance with the TRKM-C model.
2. We assess the performance of the proposed TRKM-C model by altering the values of η and σ . Fig. 2 shows significant variations in model ACC across different combinations of η and σ , underscoring the sensitivity of the proposed TRKM-C model to these hyperparameters. We can see from the results shown in Figs. 2a and 2b that the proposed TRKM-C model performs well within γ ranges of 10^{-3} to 10^5 . Fig 2c shows an increase in testing ACC within the η range of 10^{-1} to 10^5 and the σ range of 2^{-3} to 2^3 . Similarly, Fig. 2d shows that testing ACC increases as η ranges from 10^{-5} to 10^{-1} across all ranges of σ . Therefore, it is essential to carefully select the hyperparameters for the TRKM-C model to attain optimal generalization performance.

5.4. Experiments on Real World Regression Datasets

In this subsection, we evaluate the performance of the proposed TRKM-R model using 10 benchmark regression datasets from the UCI repository [35] against baseline SVR [16], TSVR [19], TSVQR [22], and RKM [28] models. Table 3 presents the detailed results of the proposed TRKM-R model and the existing models (SVR, TSVR, TSVQR, and RKM), evaluated using metrics such as *RMS E*, *MAE*, *Pos Error*,

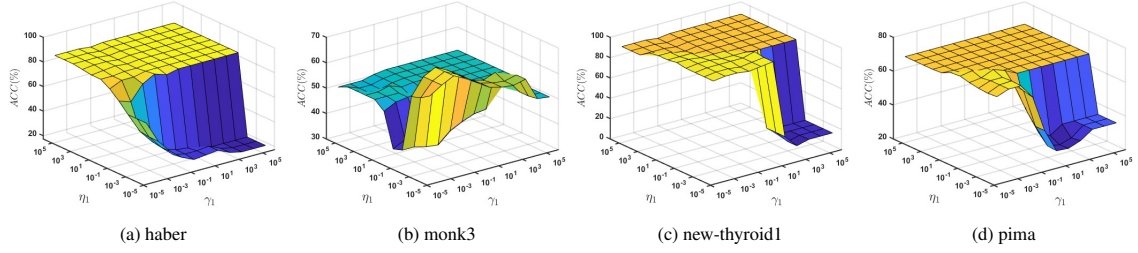


Figure 1: The impact of changing the parameters η and γ on the ACC values of the proposed TRKM-C model.

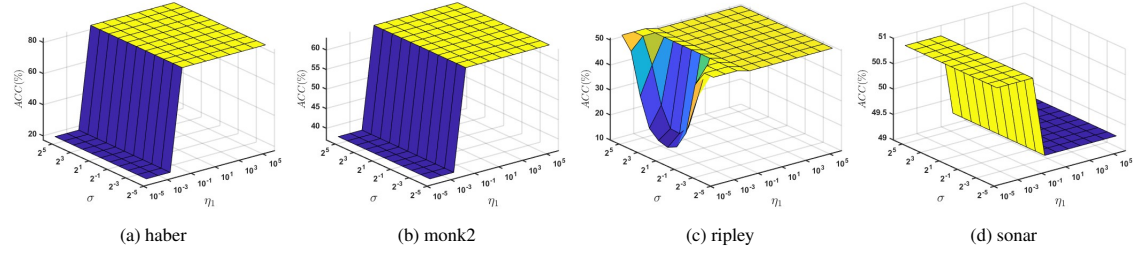


Figure 2: The impact of changing the parameters η and σ on the ACC values of the proposed TRKM-C model.

and *Neg Error. RMSE*, an important statistic whose lower values indicate better model performance, is the primary focus of the evaluation. In 7 of the 10 datasets, the proposed TRKM-R model achieves the lowest *RMSE* values, indicating superior performance. For the remaining 3 datasets, TRKM-R ranks second in terms of *RMSE*. This consistent performance across a wide range of datasets highlights the strength of the TRKM-R model. The effectiveness of the TRKM-R model is further confirmed by its average *RMSE* values. The average *RMSE* values for the existing SVR, TSVR, TSVQR, and RKM models are 0.07662296, 0.28725999, 0.81334001, and 0.0016327, respectively. In comparison, the proposed TRKM-R model achieves a superior average *RMSE* of 0.00084411, outperforming the baseline models. To evaluate model performance accurately, it is important to rank each model separately for every dataset, rather than relying solely on the average *RMSE* values. Table 3 displays the average ranking of the proposed TRKM-R model compared to the baseline models. Models are ranked based on *RMSE*, with the lowest *RMSE* receiving the highest rank. The average ranks of TRKM-R model and the existing SVR, TSVR, TSVQR, and RKM models are 1.3, 3.2, 4, 4.8, and 1.7, respectively. The rankings show the TRKM-R model's improved performance, decisively outperforming the baseline models. We conducted the Friedman test [39] and the Nemenyi post hoc test to further evaluate the efficacy of the proposed TRKM-R model. The significance of the performance variations between the models is statistically evaluated using the Friedman test. For $p = 5$ and $N = 10$, we obtained $\chi_F^2 = 35.44$ and $F_F = 69.947$. The F_F statistic follows an F -distribution with degrees of freedom (4, 36). According to the statistical F -distribution table, the critical value for $F_F(4, 36)$ at a 5% significance level is 2.6335. Since the calculated F_F value

Table 3: *RMS E*, *MAE*, *Pos Error*, and *Neg Error* values of the proposed TRKM-R and the baseline models across regression datasets.

Dataset ↓ Model → (#Samples × #Feature)		SVR [16]	TSVR [19]	TSVQR [22]	RKM [28]	TRKM-R [†]
Abalone (4117 × 7)	<i>RMS E</i>	0.00619696	0.38767592	0.07666791	0.00044776	0.00003633
	<i>MAE</i>	0.00448455	0.25410483	6.07666478	0.00000301	0.00002449
	<i>Pos Error</i>	0.00327	0.26615116	1.20577705	0.00000309	0.00001841
	<i>Neg Error</i>	0.0063161	0.00007567	6.07666478	0.00000293	0.00002719
Airfoil_Self_Noise (1503 × 5)	<i>RMS E</i>	0.28273723	0.00088726	0.25334222	0.00033556	0.00054951
	<i>MAE</i>	0.20323196	0.28901812	0.20892536	0.00000518	0.00053706
	<i>Pos Error</i>	0.30709839	0.22327934	0.32777245	0.00000503	0.00053843
	<i>Neg Error</i>	0.13613576	0.76480796	0.17763229	0.00000535	0.00033233
auto-original (392 × 7)	<i>RMS E</i>	0.02208954	0.33117149	0.66636073	0.00039196	0.00026814
	<i>MAE</i>	0.01923475	0.0577438	0.52216993	0.00022567	0.00018836
	<i>Pos Error</i>	0.02076571	0.03669568	0.58268115	0.00032394	0.00022018
	<i>Neg Error</i>	0.00786152	0.24246004	0.25812095	0.00082211	0.00010973
Auto-price (159 × 15)	<i>RMS E</i>	0.24931086	0.38767592	0.80669028	0.00047829	0.00043308
	<i>MAE</i>	0.19605144	0.07397557	0.50818611	0.00062508	0.00031579
	<i>Pos Error</i>	0.2362126	0.12724069	0.57794927	0.00018158	0.00016123
	<i>Neg Error</i>	0.07556795	0.32188751	0.32036222	0.00013476	0.00038605
bodyfat (252 × 14)	<i>RMS E</i>	0.04248758	0.1320877	0.7909357	0.0003355	0.00074434
	<i>MAE</i>	0.03476774	0.06042572	0.62823812	0.00084039	0.00060215
	<i>Pos Error</i>	0.03072008	0.08347705	0.59351638	0.00079833	0.00064703
	<i>Neg Error</i>	0.03712887	0.06934175	0.65488504	0.00057252	0.00036282
cpu_pref (209 × 9)	<i>RMS E</i>	0.04585881	0.27085771	1.40835874	0.00476195	0.0013733
	<i>MAE</i>	0.03447315	0.08627122	0.5221133	0.00033116	0.00098835
	<i>Pos Error</i>	0.02909847	0.09582179	0.68427341	0.00044175	0.00152845
	<i>Neg Error</i>	0.04264265	0.03893273	0.21990582	0.0002631	0.00086121
Daily_Demand_Forecasting_Orders (60 × 12)	<i>RMS E</i>	0.03665407	0.09586042	1.08419387	0.00294797	0.00195928
	<i>MAE</i>	0.02895825	0.06542136	0.67679833	0.00109839	0.00109826
	<i>Pos Error</i>	0.03217199	0.11739298	0.86489816	0.00176665	0.00180286
	<i>Neg Error</i>	0.01770995	0.03737439	0.30059867	0.00043014	0.00039365
gas_furnace2 (293 × 6)	<i>RMS E</i>	0.03371765	0.13730804	0.66500792	0.00003184	0.00023341
	<i>MAE</i>	0.02870417	0.6032496	0.54300641	0.00002163	0.00014806
	<i>Pos Error</i>	0.03374757	0.91916708	0.63810399	0.00020692	0.00004956
	<i>Neg Error</i>	0.0255287	0.07110268	0.49128667	0.00002272	0.00015791
machine (209 × 9)	<i>RMS E</i>	0.04578493	0.25929231	1.42404944	0.00636192	0.00264685
	<i>MAE</i>	0.03507087	0.00006935	0.57988418	0.00041585	0.00191738
	<i>Pos Error</i>	0.03397687	0.00006611	0.94066641	0.00056675	0.00251774
	<i>Neg Error</i>	0.03684863	0.02890076	0.25190033	0.00253411	0.00143709
wpbc (194 × 34)	<i>RMS E</i>	0.00139195	0.86978316	0.95779329	0.00023423	0.00019688
	<i>MAE</i>	0.00133402	0.71006265	0.63237936	0.00060265	0.00009768
	<i>Pos Error</i>	0.00125402	0.66320246	1.31818329	0.00075996	0.00009044
	<i>Neg Error</i>	0.00219808	0.45318878	0.3771965	0.00005219	0.00010569
Average <i>RMS E</i>	0.07662296	0.28725999	0.81334001	0.0016327	0.00084411	
Average rank	3.2	4	4.8	1.7	1.3	

[†] represents the proposed models.

exceeds 2.6335, the null hypothesis is rejected, indicating significant differences exist among the models. To identify significant differences in the pairwise comparisons between the models, the Nemenyi post-hoc test is used. We compute the *C.D.* as 1.1364, which means that for the average rankings in Table 3 to be deemed statistically significant, there must be a minimum difference of 1.1364 between them. The average rank distinctions between the TRKM-R model and the existing SVR, TSVR, TSVQR, and RKM models are 1.90, 2.70, 3.50, and 0.40, respectively. The proposed TRKM-R model is statistically better than other baseline models, except RKM, according to the Nemenyi post hoc test. The lower ranks of the proposed TRKM-R model indicate its stronger generalization capability compared to the existing RKM model. The combination of elevated average *RMS E* and consistent performance across multiple statistical tests provides strong evidence that the proposed TRKM-R model exceeds the performance of the existing baseline

models in terms of generalization.

5.5. Evaluation on Brain Age Prediction

In this subsection, we perform experiments on a brain age estimation dataset. The dataset comprises structural MRI scans from a total of 976 subjects, which were sourced from two prominent repositories: the OASIS dataset¹ and the IXI dataset². The OASIS dataset provides MRI data for aging studies, while the IXI dataset includes diverse brain imaging data from different age groups. This comprehensive dataset enables robust evaluation and validation of the proposed TRKM-R model for predicting brain age. The dataset consists of 30 patients diagnosed with Alzheimer’s disease (AD), 876 cognitively healthy (CH) individuals, and 70 patients with mild cognitive impairment (MCI) [40]. For training the brain age predictor, 90% of the cognitively healthy subjects were randomly selected, totaling 788 individuals with a mean age of 47.40 ± 19.69 years. For model validation, we used the remaining cognitively healthy subjects, amounting to 88 individuals with a mean age of 48.17 ± 17.73 years, along with the MCI patients (70 subjects with a mean age of 76.21 ± 7.18 years) and AD patients (30 subjects with a mean age of 78.03 ± 6.91 years). The structural MRI scans were pre-processed using the CAT12 package³ and SPM12 software⁴. Initially, the MRI scans are divided into their fundamental components: white matter (WM), gray matter (GM), and cerebrospinal fluid (CSF). This paper specifically concentrates on the GM data. The GM images are registered to the Montreal Neurological Institute (MNI) template using a diffeomorphic registration algorithm, after which they are modulated to conform to the template. A Gaussian smoothing filter with a full-width half-maximum (FWHM) of 4 millimetres is used to further process the smoothed GM pictures after they have been resampled to an isotropic spatial resolution of 8 millimetres. As a result of this process, each subject yields approximately 3,700 GM voxel values. To evaluate the prediction accuracy of the models, we compute several metrics: root mean square error (*RMS E*), mean absolute error (*MAE*), coefficient of determination (R^2), brain-age delta (Δ), and the 95% confidence interval (CI). After training each model on the training set, it is then used to estimate brain age for the independent test sets.

5.5.1. Experimental Results on the Training Set

Table 4 shows the performance of the proposed TRKM-R and the baseline models on the training set. The prediction accuracy shows that the SVR model has an *MAE* of 7.41 years, followed by the TSVR, TSVQR, and RKM models are 6.83, 6.27, and 4.79 years, and the proposed TRKM-R with 3.27 years.

¹<https://sites.wustl.edu/oasisbrains/>

²<https://brain-development.org/ixi-dataset/>

³<http://dbm.neuro.uni-jena.de/>

⁴<https://www.fil.ion.ucl.ac.uk/spm/>

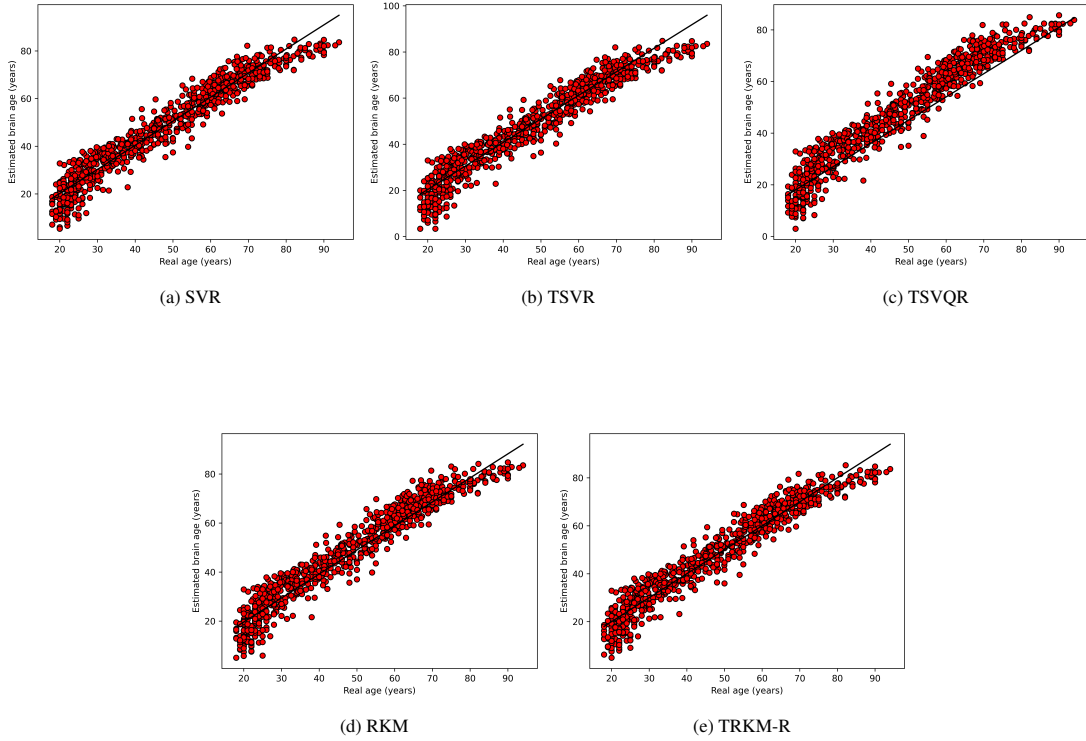


Figure 3: Real age versus estimated brain age on the training data using different prediction models, with the identity line represented by a black line.

Table 4: Comparison of the proposed TRKM-R model’s performance against baseline models using training data of Brain Age estimation.

Model →	SVR [16]	TSVR [19]	TSVQR [22]	RKM [28]	TRKM-R [†]
<i>MAE</i>	7.41	6.83	6.27	4.79	3.27
<i>RMSE</i>	8.79	7.11	6.79	5.33	3.92
Mean brain age delta	0	0	0	0	0
95% CI Values	[-0.54, 0.54]	[-0.52, 0.52]	[-0.54, 0.54]	[-0.44, 0.44]	[-0.29, 0.29]
<i>R</i> ² Score	0.88	0.88	0.88	0.92	0.96

[†] represents the proposed models.

RMSE values show a similar pattern, with the SVR model at 8.79 years, the TSVR, TSVQR, and RKM models at 7.11, 6.79, and 5.33 years, respectively, and the proposed TRKM model achieving 3.92 years. As illustrated in Table 4, the proposed TRKM-R model outperforms the existing SVR, TSVR, TSVQR, and RKM models. For all prediction models in the training set, the average brain age delta is zero. The training set’s predicted outcomes for each model failed to demonstrate a statistically significant age dependence ($P > 0.05$). Fig. 3 illustrates the relationship between the actual age and estimated brain age for different prediction models in the training set. As shown in Fig. 3, the proposed TRKM-R significantly outperformed the baseline models. The SVR, TSVR, and TSVQR models have similar prediction R^2 scores ($R^2 = 0.88$), while the RKM model has an R^2 of 0.92. In contrast, the proposed TRKM model achieved a significantly

higher R^2 of 0.96 on the same data.

5.5.2. Experimental Results on Independent Test Sets

Table 5: Comparison of the proposed TRKM-R model’s performance against baseline models using testing Data (AD, CH, and MCI subjects).

Dataset ↓ Model →		SVR [16]	TSVR [19]	TSVQR [22]	RKM [28]	TRKM-R [†]
AD	<i>MAE</i>	8.38	8.82	7.85	9.67	7.67
	<i>RMS E</i>	12.64	11.46	11.96	8.89	8.49
	Mean brain age delta	7.64	5.01	6.96	6.55	5.75
	95% CI Values	[8.22, 13.06]	[8.26, 12.77]	[6.54, 13.38]	[8.85, 14.25]	[3.85, 9.25]
	R^2 Score	0.24	0.3	0.12	0.21	0.31
CH	<i>MAE</i>	14.77	9.33	12.45	7.84	5.32
	<i>RMS E</i>	7.65	5.94	8.81	6.12	5.74
	Mean brain age delta	0.78	1.03	-3.9	1.18	1.18
	95% CI Values	[-1.54, 2.98]	[-1.58, 1.51]	[-1.15, 1.66]	[-2.89, 1.35]	[-2.72, 0.36]
	R^2 Score	0.87	0.84	0.97	0.59	0.84
MCI	<i>MAE</i>	8.82	8.6	7.84	8.98	7.31
	<i>RMS E</i>	9.69	11.84	14.14	9.03	7.03
	Mean brain age delta	4.82	4.31	4.14	4.97	3.97
	95% CI Values	[-5.53, 3.11]	[-5.75, 2.38]	[-5.85, 2.42]	[-5.13, 2.08]	[-5.13, 2.08]
	R^2 Score	0.32	0.22	0.13	0.23	0.97

[†] represents the proposed models.

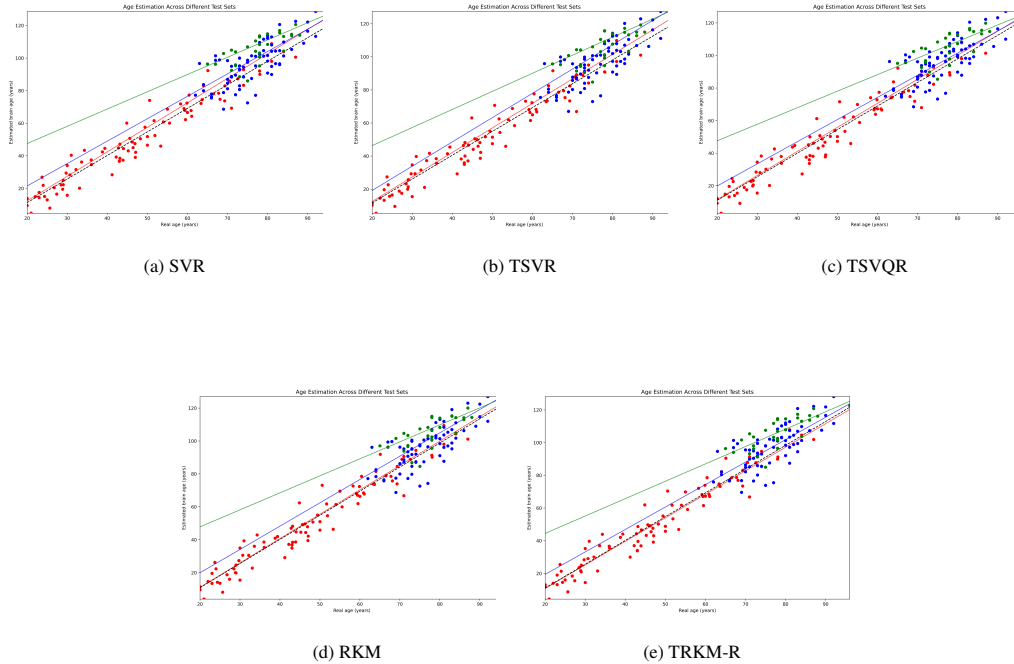


Figure 4: Estimated actual age versus brain age on the independent test sets features red markers and regression lines for CH subjects, blue markers, and regression lines for MCI subjects, and green markers and regression lines for AD subjects. An identity line, shown in black, serves as a reference for comparison across different prediction models.

Table 5 shows the performance of TRKM-R model against the baseline models on independent test sets. TRKM-R model attained an *MAE* of 5.32 years on cognitively healthy subjects, significantly outperforming the SVR, TSVR, TSVQR, and RKM models, which had *MAEs* of 14.77, 9.33, 12.45 and 7.84

years, respectively. In the independent group of cognitively healthy individuals, the mean brain age delta was approximately zero across all prediction models. The analysis of independent test sets reveals that the predicted brain age for cognitively healthy individuals did not exhibit significant age dependency across different models ($P > 0.05$), consistent with the training set results. In contrast, both AD and MCI groups showed a positive brain age delta across all models, indicating that their predicted brain age was higher than their actual age. For the MCI group, the mean brain age delta values ranged from $\Delta = 3.97$ years (TRKM-R) to $\Delta = 4.97$ years (RKM), while for the AD group, the values ranged from $\Delta = 5.75$ years (TRKM-R) to $\Delta = 7.64$ years (SVR). These results suggest that the TRKM-R model offers a lower brain age delta compared to most baseline models, reflecting better performance in brain age estimation. Fig. 4 illustrates the correlation between predicted and actual brain ages, where different markers and regression lines for CH, MCI, and AD subjects show how well the models estimate brain age across these conditions.

All prediction models revealed a positive brain age delta for both MCI and AD subjects, as shown in Table 5. This positive delta indicates that these individuals, on average, show an accelerated brain aging process compared to age-matched healthy controls. A higher brain age delta correlates with increased brain atrophy and deterioration in cognitive functions such as memory, attention, and problem-solving skills in individuals with AD [41]. This implies that MCI and AD patients generally experience more substantial brain atrophy than their healthy peers.

Specifically, individuals with AD exhibit a greater brain age delta compared to those with MCI, suggesting that AD is associated with more pronounced brain atrophy. The greater delta observed in AD patients relative to MCI patients points to a more rapid progression of brain aging in AD [41]. Furthermore, as illustrated in Fig. 4, younger patients with MCI or AD show a larger brain age discrepancy than older patients within the same diagnostic category. This finding aligns with other studies suggesting that early-onset AD patients typically exhibit a larger brain age gap compared to those with late-onset AD. The proposed TRKM-R model achieved an *MAE* of 5.32 years when applied to cognitively healthy subjects [42].

6. Conclusion

In this paper, we proposed a novel twin restricted kernel machine (TRKM) model for classification and regression. TRKM model effectively tackles the challenges related to generalization in RKMs, especially when working with unevenly distributed or complexly clustered data. By integrating the strengths of twin models and leveraging the conjugate feature duality based on the Fenchel-Young inequality, TRKM offers a robust and efficient framework for both classification and regression tasks. We evaluated the proposed

TRKM model using benchmark datasets from UCI and KEEL repositories and compared its performance against five state-of-the-art models for classification and regression. The results emphasize the outstanding performance of the TRKM model, which emerged as the top-performing model, achieving an average accuracy improvement of up to 0.42% over the second-highest baseline model. Also, our proposed TRKM model demonstrates exceptional performance for regression tasks. Statistical analyses—encompassing ranking, the Friedman test, the Nemenyi post hoc test, and the win-tie-loss sign test—demonstrate that our proposed model significantly outperforms the baseline models in terms of robustness. Additionally, the efficacy of our proposed TRKM model in brain age prediction is validated, showing superior performance compared to the baseline models. While the proposed model has demonstrated exceptional performance on single-view datasets, its effectiveness in multiview scenarios has not yet been assessed. Future research should focus on adapting the TRKM model for multiview problems and exploring methods to reduce computational complexity while extending the model’s applicability to datasets with multiple views. Another potential direction is to explore the integration of more advanced kernel functions or the development of adaptive kernel strategies that can dynamically adjust to the underlying data distribution, enhancing performance in highly heterogeneous datasets. Additionally, exploring the application of TRKM in unsupervised learning tasks, such as clustering and dimensionality reduction, could reveal new insights and broaden its utility.

Acknowledgement

This study receives support from the Science and Engineering Research Board (SERB) through the Mathematical Research Impact-Centric Support (MATRICS) scheme Grant No. MTR/2021/000787. The authors gratefully acknowledge the invaluable support provided by the Indian Institute of Technology Indore.

References

- [1] Corinna Cortes and Vladimir Vapnik. Support-vector networks. *Machine Learning*, 20:273–297, 1995.
- [2] Mahesh Pal and Paul M Mather. Support vector machines for classification in remote sensing. *International Journal of Remote Sensing*, 26(5):1007–1011, 2005.
- [3] Bharat Richhariya and M. Tanveer. EEG signal classification using universum support vector machine. *Expert Systems with Applications*, 106:169–182, 2018.

- [4] A Quadir and M Tanveer. Granular ball twin support vector machine with pinball loss function. *IEEE Transactions on Computational Social Systems*, 2024, 10.1109/TCSS.2024.3411395.
- [5] Yuanqing Li and Cuntai Guan. Joint feature re-extraction and classification using an iterative semi-supervised support vector machine algorithm. *Machine Learning*, 71:33–53, 2008.
- [6] Johan AK Suykens and Joos Vandewalle. Least squares support vector machine classifiers. *Neural Processing Letters*, 9:293–300, 1999.
- [7] Olvi L Mangasarian and Edward W Wild. Multisurface proximal support vector machine classification via generalized eigenvalues. *IEEE Transactions on Pattern Analysis and Machine Intelligence*, 28(1):69–74, 2005.
- [8] Jayadeva, Reshma Khemchandani, and Suresh Chandra. Twin support vector machines for pattern classification. *IEEE Transactions on Pattern Analysis and Machine Intelligence*, 29(5):905–910, 2007.
- [9] Mohammad Tanveer, T Rajani, Reshma Rastogi, Yuan-Hai Shao, and M. A Ganaie. Comprehensive review on twin support vector machines. *Annals of Operations Research*, pages 1–46, 2022, <https://doi.org/10.1007/s10479-022-04575-w>.
- [10] A Quadir, M Sajid, M Tanveer, and P N Suganthan. Enhanced feature based granular ball twin support vector machine. *arXiv preprint arXiv:2410.05786v1*, 2024.
- [11] M Arun Kumar and Madan Gopal. Least squares twin support vector machines for pattern classification. *Expert Systems with Applications*, 36(4):7535–7543, 2009.
- [12] A Quadir and M Tanveer. Intuitionistic fuzzy universum twin support vector machine for imbalanced data. *arXiv preprint arXiv:2410.20335*, 2024.
- [13] A Quadir, M A Ganaie, and M Tanveer. Intuitionistic fuzzy generalized eigenvalue proximal support vector machine. *Neurocomputing*, 608:128258, 2024.
- [14] A Quadir and M Tanveer. Multiview learning with twin parametric margin SVM. *arXiv preprint arXiv:2408.01981*, 2024.
- [15] Abdul Quadir, Mushir Akhtar, and M Tanveer. Enhancing multiview synergy: robust learning by exploiting the wave loss function with consensus and complementarity principles. *arXiv preprint arXiv:2408.06819*, 2024.

- [16] Debasish Basak, Srimanta Pal, Dipak Chandra Patranabis, et al. Support vector regression. *Neural Information Processing-Letters and Reviews*, 11(10):203–224, 2007.
- [17] Harris Drucker, Christopher J Burges, Linda Kaufman, Alex Smola, and Vladimir Vapnik. Support vector regression machines. *Advances in neural information processing systems*, 9, 1996.
- [18] Mushir Akhtar, M Tanveer, and Mohd Arshad. Enhancing efficiency and robustness in support vector regression with hawkeye loss. *arXiv preprint arXiv:2401.16785*, 2024.
- [19] Xinjun Peng. TSVR: an efficient twin support vector machine for regression. *Neural Networks*, 23(3):365–372, 2010.
- [20] Xinjun Peng, Dong Xu, and Jindong Shen. A twin projection support vector machine for data regression. *Neurocomputing*, 138:131–141, 2014.
- [21] Yuan-Hai Shao, Chun-Hua Zhang, Zhi-Min Yang, Ling Jing, and Nai-Yang Deng. An ε -twin support vector machine for regression. *Neural Computing and Applications*, 23:175–185, 2013.
- [22] Yafen Ye, Zhihu Xu, Jinhua Zhang, Weijie Chen, and Yuanhai Shao. Twin support vector quantile regression. *Expert Systems with Applications*, 237:121239, 2024.
- [23] Yong-Ping Zhao, Jing Zhao, and Min Zhao. Twin least squares support vector regression. *Neurocomputing*, 118:225–236, 2013.
- [24] Bernhard Schölkopf and Alexander J Smola. *Learning with kernels: support vector machines, regularization, optimization, and beyond*. MIT press, 2002.
- [25] J Shawe-Taylor. Kernel methods for pattern analysis. *Cambridge University Press*, 2:181–201, 2004.
- [26] Christopher M Bishop. Pattern recognition and machine learning. *Springer*, 2:1122–1128, 2006.
- [27] Nello Cristianini and John Shawe-Taylor. *An introduction to support vector machines and other kernel-based learning methods*. Cambridge University Press, 2000.
- [28] Johan AK Suykens. Deep restricted kernel machines using conjugate feature duality. *Neural Computation*, 29(8):2123–2163, 2017.
- [29] Geoffrey E Hinton, Simon Osindero, and Yee-Whye Teh. A fast learning algorithm for deep belief nets. *Neural Computation*, 18(7):1527–1554, 2006.
- [30] R Tyrrell Rockafellar. *Conjugate Duality and Optimization*. SIAM, 1974.

- [31] Arun Pandey, Joachim Schreurs, and Johan AK Suykens. Generative restricted kernel machines: A framework for multi-view generation and disentangled feature learning. *Neural Networks*, 135: 177–191, 2021.
- [32] Arun Pandey, Michaël Fanuel, Joachim Schreurs, and Johan AK Suykens. Disentangled representation learning and generation with manifold optimization. *Neural Computation*, 34(10):2009–2036, 2022.
- [33] Lynn Houthuys and Johan AK Suykens. Tensor-based restricted kernel machines for multi-view classification. *Information Fusion*, 68:54–66, 2021.
- [34] Francesco Tonin, Panagiotis Patrinos, and Johan AK Suykens. Unsupervised learning of disentangled representations in deep restricted kernel machines with orthogonality constraints. *Neural Networks*, 142:661–679, 2021.
- [35] Dheeru Dua and Casey Graff. UCI machine learning repository. Available: <http://archive.ics.uci.edu/ml>, 2017.
- [36] J Derrac, S Garcia, L Sanchez, and F Herrera. KEEL data-mining software tool: Data set repository, integration of algorithms and experimental analysis framework. *J. Mult. Valued Log. Soft Comput.*, 17:255–287, 2015.
- [37] M. Tanveer, A. Sharma, and P. N. Suganthan. General twin support vector machine with pinball loss function. *Information Sciences*, 494:311–327, 2019.
- [38] A Quadir, M Sajid, and M Tanveer. Granular ball twin support vector machine. *IEEE Transactions on Neural Networks and Learning Systems*, 2024, 10.1109/TNNLS.2024.3476391.
- [39] Janez Demšar. Statistical comparisons of classifiers over multiple data sets. *The Journal of Machine Learning Research*, 7:1–30, 2006.
- [40] M A Ganaie, Muhammad Tanveer, and Iman Beheshti. Brain age prediction with improved least squares twin SVR. *IEEE Journal of Biomedical and Health Informatics*, 27(4):1661–1669, 2022.
- [41] Iman Beheshti, Norihide Maikusa, and Hiroshi Matsuda. The association between “Brain-Age Score”(BAS) and traditional neuropsychological screening tools in Alzheimer’s disease. *Brain and Behavior*, 8(8):e01020, 2018.
- [42] Iman Beheshti, Scott Nugent, Olivier Potvin, and Simon Duchesne. Disappearing metabolic youthfulness in the cognitively impaired female brain. *Neurobiology of Aging*, 101:224–229, 2021.